Human GDPD3 overexpression promotes liver steatosis by increasing lysophosphatidic acid production and fatty acid uptake

Chia-Chi C. Key,[1,*] Andrew C. Bishop,[*] Xianfeng Wang,[*] Qingxia Zhao,[*] Guan-yuan Chen,[†] Matthew A. Quinn,[§] Xuewei Zhu,[*] Qibin Zhang,[†] and John S. Parks[*,]**

Section on Molecular Medicine, Department of Internal Medicine,* Section on Comparative Medicine, Department of Pathology,[§] and Department of Biochemistry,** Wake Forest School of Medicine, Winston-Salem, NC 27157; and Department of Chemistry and Center for Translational Biomedical Research,[†] University of North Carolina at Greensboro, Greensboro, NC 27402

ORCID IDs: 0000-0003-0669-2936 (C-C.C.K.); 0000-0002-5227-8915 (J.S.P.)

Abstract The glycerol phosphate pathway produces more than 90% of the liver triacylglycerol (TAG). LysoPA, an intermediate in this pathway, is produced by glycerol-3-phosphate acyltransferase. Glycerophosphodiester phosphodiesterase domain containing 3 (GDPD3), whose gene was recently cloned, contains lysophospholipase D activity, which produces LysoPA from lysophospholipids. Whether human GDPD3 plays a role in hepatic TAG homeostasis is unknown. We hypothesized that human GDPD3 increases LysoPA production and availability in the glycerol phosphate pathway, promoting TAG biosynthesis. To test our hypothesis, we infected C57BL/6J mice with adeno-associated virus encoding a hepatocyte-specific albumin promoter that drives GFP (control) or FLAG-tagged human *GDPD3* overexpression and fed the mice chow or a Western diet to induce hepatosteatosis. Hepatic human *GDPD3* overexpression induced LysoPA production and increased FA uptake and incorporation into TAG in mouse hepatocytes and livers, ultimately exacerbating Western diet-induced liver steatosis. Our results also showed that individuals with hepatic steatosis have increased *GDPD3* mRNA levels compared with individuals without steatosis. Collectively, these findings indicate that upregulation of GDPD3 expression may play a key role in hepatic TAG accumulation and may represent a molecular target for managing hepatic steatosis.—Key, C-C. C., A. C. Bishop, X. Wang, Q. Zhao, G-y. Chen, M. A. Quinn, X. Zhu, Q. Zhang, and J. S. Parks. **Human GDPD3 overexpression promotes liver steatosis by increasing lysophosphatidic acid production and fatty acid uptake. *J. Lipid Res.* 2020.** 61: **1075–1086.**

Supplementary key words lipid metabolism • triacylglycerol • glycerophosphodiester phosphodiesterase domain containing 3 • glycerol phosphate pathway • hepatic steatosis • Western diet

NAFLD was first described in 1980 (1). About 75% of individuals with NAFLD have nonalcoholic fatty liver (NAFL), characterized by isolated hepatic steatosis or combined steatosis and mild nonspecific inflammation. The remaining 25% have NASH, with steatosis, mild nonspecific inflammation, and hepatocellular injury with or without hepatic fibrosis (2). Hepatic steatosis is the hallmark of NAFL/NAFLD resulting from increased triacylglycerol (TAG) acquisition and disposition in hepatocytes. Increased hepatic TAG can result from: *1*) increased uptake of plasma nonesterified FA derived from adipose tissue or diet, *2*) elevated de novo FA synthesis, *3*) increased FA esterification to form TAG, *4*) reduced FA oxidation, and/or *5*) impaired VLDL assembly and secretion (3). There are two pathways involved in TAG synthesis, the glycerol phosphate pathway and the monoacylglycerol pathway; the former is used by most cells for TAG synthesis, whereas the latter predominates in the small intestine (4). The first step of TAG synthesis in the glycerol phosphate pathway (**Fig. 1**) is FA esterification of glycerol 3-phosphate by glycerol-3-phosphate acyltransferase (GPAT) to form LysoPA (5). An additional FA is subsequently incorporated into

This work was supported by National Institutes of Health Grants DK117069, HL132035 (X.Z.), DK123499 (Q.Z.), (C-C.C.K.) and HL119962 (J.S.P.). The content is solely the responsibility of the authors and does not necessarily represent the official views of the National Institutes of Health. The authors declare that they have no conflicts of interest with the contents of this article.

Manuscript received 12 March 2020 and in revised form 13 May 2020.

Published, JLR Papers in Press, May 19, 2020
DOI https://doi.org/10.1194/jlr.RA120000760

This article is available online at https://www.jlr.org

Abbreviations: AAV, adeno-associated virus; AGPAT, 1-acylglycerol-3-phosphate acyltransferase; CE, cholesteryl ester; CPT, carnitine palmitoyltransfersase; FATP, fatty acid transporter protein; FC, free cholesterol; GDE1, glycerophosphodiester phosphodiesterase 1; GDPD3, glycerophosphodiester phosphodiesterase domain containing 3; GPAT, glycerol-3-phosphate acyltransferase; hGDPD3, human glycerophosphodiester phosphodiesterase domain containing 3; PL, phospholipid; TAG, triacylglycerol.

[1] To whom correspondence should be addressed.
e-mail: cchuang@wakehealth.edu

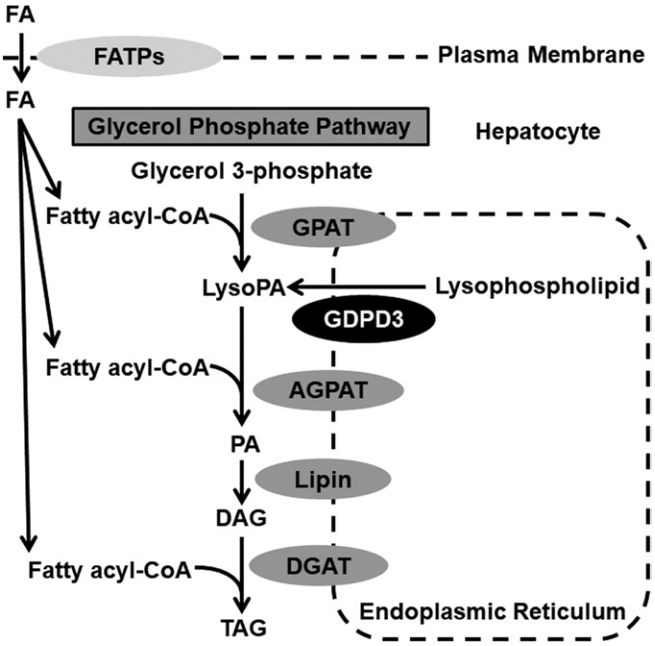

Fig. 1. Glycerol phosphate pathway for de novo TAG synthesis. DGAT, DAG acyltransferase; FATP, fatty acid transporter protein.

LysoPA, forming PA by a family of 1-acylglycerol-3-phosphate acyltransferases (AGPATs) (6). The lipin phosphatidic acid phosphatase enzymes dephosphorylate PA to synthesize DAG (7). Finally, DAG is converted to TAG through the action of DAG acyltransferase (8). The glycerol phosphate pathway primarily occurs in the ER and to a lesser extent on lipid droplets at the mitochondrial membrane and at the nuclear envelope (9).

Bacterial and fungal glycerophosphodiester phosphodiesterases (GDPDs) hydrolyze glycerophosphodiester to produce glycerol 3-phosphate (10–12); however, mammalian GDPDs have additional substrates. For example, mouse GDPD3 was recently cloned and found to be an ER membrane-associated enzyme that has lysophospholipase D activity, converting 1-acyl-lysophosphatidylcholine and 1-*O*-alkyl-*sn*-glycero-3-phosphocholine to 1-acyl-LysoPA and alkyl-LysoPA, respectively (13). LysoPA is an intermediate of the glycerol phosphate pathway for TAG synthesis in liver (Fig. 1) (14). In addition, our previous study identified the mouse GDPD3 gene as one of the the top five genes involved in liver lipid metabolism and hepatic steatosis (15). However, mammalian GDPD3 has not previously been implicated in the regulation of hepatic TAG metabolism. Therefore, this study was designed to examine whether human GDPD3 overexpression in mouse liver increases LysoPA availability for TAG synthesis through the ER glycerol phosphate pathway, leading to hepatic steatosis and to determine what the underlying mechanisms are. We reported that hepatic human GDPD3 overexpression induced LysoPA production and increased FA uptake and incorporation into TAG in mouse hepatocytes and livers, ultimately exacerbating Western diet-induced liver steatosis.

MATERIALS AND METHODS

Mice

C57BL/6J mice (Jackson Laboratory, Stock No. 000664) were housed in standard caging at 22°C in a 12 h light and 12 h dark cycle (dark from 6:00 PM to 6:00 AM) at standard temperature and humidity conditions with ad libitum access to water and a standard chow diet (Purina-LabDiet, Prolab RMH 3000). All experiments were performed using a protocol approved by the Institutional Animal Care and Use Committee at Wake Forest School of Medicine in facilities approved by the American Association for Accreditation of Laboratory Animal Care.

Gdpd3 mRNA quantification in mouse tissues

Twelve-week-old mice were fasted for 24 h (three male and three female mice), anesthetized with ketamine/xylazine, and then transcardially perfused with ice-cold 1× Dulbecco's PBS (15). Liver, visceral white adipose tissue (epididymal for male mice and periovarian for female mice), brown adipose tissue, heart, brain (cerebrum), kidney, duodenum, jejunum, ileum, and colon were snap-frozen in liquid nitrogen and stored in a −80°C freezer. mRNA abundance of *Gdpd3* was measured by real-time PCR. For a fasting/refeeding study (15), 12-week-old male mice were fasted for 24 h (n = 5), and another group was fasted for 24 h followed by refeeding a standard chow diet for 12 h (n = 5); fasting start times were staggered between groups so that both groups of mice were euthanized together. Livers were collected to measure TAG levels (Wako Diagnostics L-Type TG M) and *Gdpd3* mRNA abundance by real-time PCR.

Overexpression of hepatic human *GDPD3* in chow-fed mice

Six-week-old male mice were injected (retro-orbital; 3×10^{11} genome copies per mouse) with adeno-associated virus (AAV) serotype 8 (Vector Biolabs) encoding a hepatocyte-specific promoter (i.e., albumin) driving GFP (AAV-GFP) expression (controls; n = 6) or FLAG-tagged human *GDPD3* (AAV-hGDPD3) to overexpress human GDPD3 in mouse liver (n = 6). Mice were euthanized 18 weeks after AAV injection, after an overnight fast, and plasma and livers were harvested for lipid measurement (15). Livers were lipid extracted using a modified Folch method for measurement of LysoPA content (lipid class analysis) as reported previously (16). Liver (50 mg) was homogenized in 20 vol of extraction solvent (chloroform:methanol, 2:1, v/v) using a Precellys homogenizer (Montigny-le-Bretonneux, France) at 6,700 rpm for 15 s (repeated three times at 30 s intervals for a total of four times). The liver homogenate was incubated at 4°C for 2 h, and then the supernatant was harvested and stored at −20°C prior to analysis. Mixed mode HPLC was performed on an Agilent (Palo Alto, CA) 1200 HPLC system consisting of a quaternary pump, an autosampler, a column oven, and an evaporative light scattering detector. A Chromolith Performance Si column (100 × 4.6 mm, macropore size 2.1 μm and mesopores size 13 nm; Merck, Darmstadt, Germany) was used for class-based lipid separation following previously described gradient and separation conditions (16). Peaks for LysoPA were manually integrated. The samples were analyzed randomly with blank runs in between. LysoPA (18:1) was purchased from Avanti Polar Lipids (Alabaster, AL) and used as a standard to establish the retention time profiles in mixed mode HPLC analysis. Six calibrator concentrations ranging from 0.003125 to 0.1 mg/ml for LysoPA were employed to construct standard curves. LysoPA concentration in each sample was determined using the standard curve.

Chow-fed mice (16–18 weeks of age) were used for comprehensive systemic metabolic phenotyping including measurement of

blood glucose, plasma insulin, and plasma β-hydroxybutyrate levels after a 24 h fast followed by a 3 h chow refeeding (15). We also measured oxygen consumption (VO_2, milliliters per hour per kilogram), carbon dioxide production (VCO_2, milliliters per hour per kilogram), heat production (kilocalories per hour per kilogram), food intake (grams per 12 h), and respiratory exchange ratio (VCO_2/VO_2) of mice during a 12 h light and 12 h dark cycle for three consecutive days using a six-chamber indirect calorimetry system (PhenoMaster; TSE Systems, Bad Homburg, Germany). Data collected during the second day are presented (17).

Plasma and extracted liver lipids were used to measure TAG (Wako Diagnostics L-Type TG M), free cholesterol (FC) (Wako Free Cholesterol E), total cholesterol (Wako Cholesterol E), and total phospholipids (PLs) (Wako Phospholipids C) using enzymatic assays (15). Cholesteryl ester (CE) was calculated using the equation (TAG − FC) × 1.67 (18). The nonextractable liver residue was air-dried and solubilized with 0.1 N of NaOH to quantify liver protein content using the Lowry method (19).

Hepatic LysoPA production

Twelve-week-old male mice were administered AAV-GFP or AAV-hGDPD3. After 6–10 weeks of AAV injection, primary hepatocytes from chow-fed mice were isolated (see the section of Primary hepatocyte isolation below) and treated with [1-^{14}C]palmitic acid (PerkinElmer #NEC075H) at 0.5 μCi [1-^{14}C]palmitic acid per milliliter of medium for 0, 1, 2, and 4 h. Following radiolabeling, cells were washed with ice-cold Dulbecco's PBS twice and lipid-extracted with hexane:isopropanol (3:2, v/v). After lipid extraction, cell residue was dissolved with 0.1 N of NaOH and protein concentrations were measured using a Pierce™ BCA protein assay kit for protein normalization of data. Lipid classes from standards and cell lipid extracts were separated by TLC using silica gel plates and a solvent system containing chloroform:methanol:20% ammonia (60:35:8, v/v/v) (13). Lipids were visualized by exposure to iodine vapor, and bands corresponding to LysoPA were scraped and counted using a scintillation counter. Two biological experiments were conducted on separate days. In each experiment, primary hepatocytes were isolated from one mouse per genotype and n = 6 per time point.

Primary hepatocyte isolation

The procedure of primary hepatocyte isolation was described previously (15). Mouse primary hepatocytes were seeded at $0.5–1 \times 10^6$ per well in a 6-well plate containing William's E medium (Life Technologies #12551-032) supplemented with antibiotics, including 100 IU/ml of penicillin and 100 μg/ml of streptomycin (Life Technologies #15140-122). After 2–3 h of cell attachment at 37°C under 5% CO_2, hepatocytes were cultured in William's E medium supplemented with antibiotics, 10% fetal bovine serum, and indicated tracers labeled with radioactive isotopes.

Overexpression of hepatic human *GDPD3* in mice on a Western diet

Six-week-old male mice were injected with AAV-GFP (n = 15) or AAV-hGDPD3 (n = 15). Two weeks later, the mice were switched from a standard rodent chow to a Western diet (Envigo #TD88137; 42% fat calories, 0.2% cholesterol) for 12 weeks to induce obesity, insulin resistance, and hepatic steatosis (15). Mice were used for a comprehensive systemic metabolic phenotyping between 8 and 10 weeks of Western diet feeding as described above. Mice were also fasted for 16 h for an intraperitoneal glucose tolerance test (Sigma-Aldrich #G7528) (1 g/kg body weight) or fasted for 4 h for an intraperitoneal insulin tolerance test (Eli Lilly and Co. Humulin RU-100) (0.75 U/kg body weight).

AAV-injected mice were euthanized after 12 weeks of Western diet feeding and an overnight fast and plasma and liver were harvested for lipid measurements as described above. Untargeted lipidomic analysis of liver LysoPA species was also performed. Liver (100 mg) was homogenized in 500 μl of chilled chloroform:methanol (2:1, v/v) using a Bead Mill homogenizer (Bead Ruptor; Omni International, Kennesaw, GA). The organic extract was collected after pelleting extracted liver at 16,000 *g* for 5 min and dried under a stream of nitrogen at room temperature. The lipid extracts were solubilized with 100 μl of isopropyl alcohol:methanol (1:1, v/v) for LC-MS/MS analysis. High-resolution LC-MS/MS analysis was performed on a Q Exactive HF hybrid quadrupole-Orbitrap mass spectrometer (Thermo Scientific, Waltham, MA) with heated ESI source and a Vanquish UHPLC system (Thermo Scientific) (20). Lipids were separated on an Accucore C30 column (2.6μm, 3 × 150 mm) using a linear gradient with acetonitrile:water (60:40, v/v) (mobile phase A) and isopropyl alcohol:acetonitrile (90:10, v/v) (mobile phase B), both of which contained 0.1% formic acid and 10 mM ammonium formate. LysoPA (16:0), LysoPA (18:0), and LysoPA (18:1) standards were used to verify the LysoPA peaks based on the peak fragmentation and retention times. LipidSearch 4.2 software (Thermo Scientific) was used for lipid identification and quantitation. The LC-MS data containing high-resolution MS and data-dependent MS/MS were searched using the parameters as follows: precursor mass tolerance, 5 ppm; product mass tolerance, 5 ppm; PL species selection, LysoPA.

Primary hepatocytes were isolated from Western diet-fed mice (8–10 weeks of feeding) and used to study de novo TAG biosynthesis using [1-^{14}C]acetic acid (PerkinElmer #NEC084A001MC), FA esterification into TAG using [9,10-^{3}H(N)]oleic acid (PerkinElmer #NET289005MC), FA uptake using [1-^{14}C]palmitic acid as described previously (15). In each study, three to five biological experiments were conducted on separate days. In each experiment, primary hepatocytes were isolated from one mouse per genotype and three incubation time points were investigated (n = 3 per time point).

Patient liver samples

This study was approved by the Institutional Review Board (IRB00010545) at Wake Forest School of Medicine. The study abides by the Declaration of Helsinki principles. Patients undergoing Roux-en-Y gastric bypass, lap band, cholecystectomy, hernia repair, or other abdominal surgery were approached for informed consent to collect fasting blood samples (just prior to surgery) and one intraoperative liver biopsy during their procedure. The main inclusion criteria for participation were age 21–80 years and intent to undergo an elective abdominal surgery with the visualization of the liver at Wake Forest University Baptist Medical Center (Winston-Salem, NC). Exclusion criteria were positive hepatitis C antibody or hepatitis B surface antigen, cirrhosis or chronic liver disease (other than NAFLD), past or present malignancy (other than nonmelanoma skin cancer), or need for chronic anticoagulation. Over the course of the study, 54 subjects were recruited; no vulnerable populations were included. Fasting blood samples were used for glucose and insulin levels as well as plasma lipid profiles as described above. The liver biopsy was a resection of hepatic tissue taken with a scalpel as well as a core needle biopsy. The liver tissue was divided in the operating room into two samples. One portion (∼0.5–1 g) was immediately snap-frozen in liquid nitrogen for liver lipid profiles and RNA/cDNA extraction for GDPD3 gene expression by real-time PCR. The second portion of the liver sample (needle core biopsy) was fixed in 10% buffered formalin and submitted to surgical pathology for histopathologic characterization by a certified pathologist at Wake Forest University Baptist Medical Center. Briefly, hematoxylin and eosin and trichrome slide preparations were

performed per center standards (21). A semiquantitative measure of macro-steatosis was made by point counting hepatocytes at 4,009 optical magnification. An overlying grid of 35 μm^2 boxes was used to assist counting. The hepatocytes of five nonoverlapping fields that did not include a portal tract were hand counted, yielding percentages of hepatocytes as macro-steatotic (lipid droplets large enough to displace the nucleus and/or ⩾15 μm) and normal (no evidence of lipid droplets) (22). Degrees of macro-steatosis were graded according to the convention established by Kleiner et al. (23) including: <5% of macro-steatosis, grade 1; ⩾5% to <30% of mild macro-steatosis, grade 2; ⩾30% to ⩽60% of moderate macro-steatosis, grade 3; >60% of severe macro-steatosis, grade 4.

Real-time PCR analysis

Total RNA was isolated from hepatocytes and tissues using QIAzol lysis buffer (Qiagen #79306) and RNeasy Plus universal kit (Qiagen #73404). cDNA synthesis was performed with an Omniscript RT kit (Qiagen #205113) using 1 μg of RNA. Real-time PCR was performed using TaqMan® gene expression assays (Thermo Fisher Scientific #4331182) to measure *GDPD3* (Hs00225626_m1), *Gdpd3* (Mm00470322_m1), *Fasn* (Mm00662319_m1), acetyl-CoA carboxylase (*Acc*) 1 (Mm01304257_m1), *Gpat4/Agpat6* (Mm00497622_m1), *Pparα* (Mm00440939_m1), carnitine palmitoyltransfersase (*Cpt*) *Iα* (Mm00440939_m1), and *Cpt2* (Mm00487205_m1). Gene expression was normalized to the housekeeping gene *Gapdh* (Mm99999915_g1) or 18S rRNA (Thermo Scientific #4352930E) and analyzed using the ΔΔ-CT method with 95% confidence (24).

Immunoblotting

Mouse tissues were lysed in RIPA lysis buffer (Thermo Scientific #89900) containing protease inhibitor cocktail (Roche #05892791001) and homogenized in 1.4 mm prefilled ceramic bead tubes (Fisher Scientific #15340153) for 15 s at 2,200 rpm for soft tissues (i.e., liver, adipose tissue, brain, and kidney) or in 2.4 mm prefilled ceramic bead tubes (Fisher Scientific #15340151) for 30 s at 2,200 rpm for hard tissues (i.e., heart and intestines) using a bead beater (Biospec Mini-BeadBeater-96). After centrifugation of tubes at 12,000 *g* for 15 min at 4°C, the supernatant proteins were fractioned by 4–20% Criterion TGX precast gels (Bio-Rad #5671094) and transferred to a polyvinylidene fluoride membrane. Membranes were blocked with 5% nonfat dry milk in TBS with 0.1% Tween-20 (TBST), incubated with primary antibody at 4°C overnight, washed three times with TBST, and then incubated with secondary antibody for 1 h at room temperature. Blots were incubated with SuperSignal West Pico chemiluminescence substrate (Pierce) and visualized with a ChemiDoc MP imaging system (Bio-Rad). Primary antibodies used for immunoblots included the following: GDPD3 (custom made by Lampire Biological Laboratories, 1 μg/ml buffer), GFP (Cell Signaling #2956S, 1:1,000), FLAG (Sigma-Aldrich #F1804, 1:1,000), and GAPDH (Santa Cruz #32233, 0.02 μg/ml), which was used as a loading control. Secondary antibodies used for immunoblots were HRP-conjugated anti-mouse (Santa Cruz, 1:10,000) and anti-rabbit (GE Healthcare, 1:10,000).

Statistics

Results are presented as mean ± SEM. Data were analyzed using a two-tailed Student's unpaired *t*-test for cell and mouse studies or unpaired *t*-test with Welch's correction for the human study, or two-way ANOVA with Sidak multiple comparisons. All analyses were performed using GraphPad Prism 7 software. A *P*-value of 0.05 was used as the cutoff for statistical significance.

RESULTS

Endogenous GDPD3 gene expression

GDPD belongs to a highly conserved family of enzymes (12). The GDPD3 gene is conserved in human, chimpanzee, rhesus monkey, dog, cow, rat, mouse, zebrafish, and frog. Human GDPD3 is a 318 amino acid protein that shares 78.9% sequence identity with mouse (330 amino acids) and 76.9% with rat (331 amino acids) orthologs. We measured Gdpd3 expression across multiple tissues from male and female C57BL/6J mice after a 24 h fast. Gdpd3 mRNA abundance was relatively low (Ct 29–33) in all tissues examined and was not affected by the sex of the mice (**Fig. 2A**). We also found that livers displayed relatively low endogenous Gdpd3 mRNA expression (Fig. 2A). Previous studies reported that livers of C57BL/6J mice accumulated

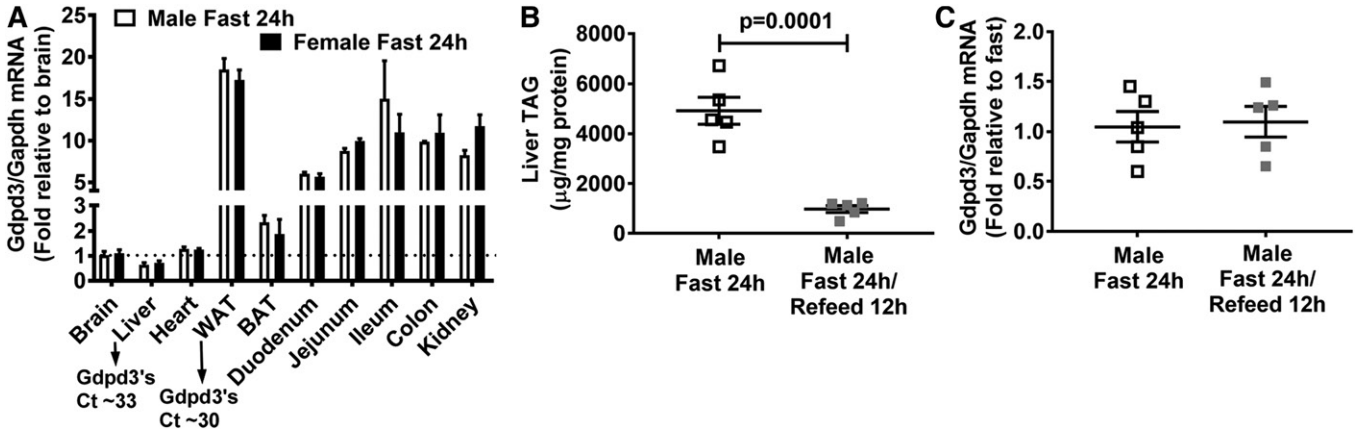

Fig. 2. GDPD3 gene expression in mouse tissues. Twelve-week-old mice were fasted for 24 h (three male and three female) and tissues were harvested for measurement of Gdpd3 mRNA levels by real-time PCR (A). In a second study, 12-week-old male mice were fasted for 24 h (n = 5), and another group was fasted for 24 h followed by refeeding a standard chow diet for 12 h (n = 5); fasting times were staggered so that both groups of mice were euthanized together. Livers were collected to measure TAG levels (B) and Gdpd3 mRNA levels (C) by real-time PCR. All results are mean ± SEM and analyzed using a two-tailed Student's unpaired *t*-test. Ct, cycle threshold; WAT, white adipose tissue; BAT, brown adipose tissue.

large amounts of TAG (a 4- to 14-fold increase) after fasting for 6–24 h (25, 26). Indeed, we observed that fasting significantly increased liver TAG content (Fig. 2B) but did not modify Gdpd3 mRNA levels compared with refeeding (Fig. 2C). These data suggest that GDPD3 does not play a role in liver TAG homeostasis in response to fasting and fasting/refeeding status.

Overexpression of human GDPD3 in mouse liver increases hepatic LysoPA content but does not affect hepatic TAG content in chow-fed mice

Previous studies reported that recombinant mouse and human GDPD3 is an ER membrane-associated enzyme that contains lysophospholipase D activity, hydrolyzing lysophospholipids to produce LysoPA in nonhepatic cell lines (13, 27). Because LysoPA is an intermediate in the ER glycerol phosphate pathway for TAG synthesis (14), we hypothesized that human GDPD3 increases LysoPA substrate, promoting hepatic TAG biosynthesis and accumulation. To test our hypothesis, we performed a lipid class analysis using livers isolated from chow-fed mice injected with AAV encoding a hepatocyte-specific promoter (i.e., albumin) driving FLAG-tagged human *GDPD3* (AAV-hGDPD3) or GFP (AAV-GFP) as control. There was no difference in mouse endogenous liver Gdpd3 mRNA expression between AAV-GFP- and AAV-hGDPD3-injected mice (**Fig. 3A**). Human GDPD3 overexpression in mouse liver was verified at protein levels (Fig. 3B). No expression of human GDPD3 was observed in adipose tissue and muscle, indicating the specificity of human GDPD3 expression in mouse liver (Fig. 3C). Hepatic LysoPA content was increased ~2-fold with human GDPD3 overexpression compared with GFP controls (Fig. 3D).

To confirm the data of liver lipid class analysis (Fig. 3D), we isolated primary hepatocytes from chow-fed mice and treated the cells with [^{14}C]palmitic acid. The production of [^{14}C]LysoPA from [^{14}C]palmitic acid increased in primary hepatocytes overexpressing human GDPD3 compared with GFP controls in a time-dependent manner (Fig. 3E). Overexpression of human GDPD3 in mouse primary hepatocytes did not affect mouse endogenous Gdpd3 mRNA levels (Fig. 3F) and was verified by increased human GDPD3 protein levels (Fig. 3G).

We then examined whether increased hepatic LysoPA content affected hepatic lipid content and systemic metabolism because our previous study suggested an association between dysregulated hepatic lipid metabolism and impaired systemic metabolic phenotype (15). We observed that mice overexpressing human GDPD3 in liver had increased plasma LysoPA levels (**Fig. 4A**) but had normal circulating (Fig. 4B) and hepatic (Fig. 4C) lipid concentrations and content, respectively, compared with GFP control mice. There was also no difference in systemic metabolic phenotypes including body weight (Fig. 4D), blood glucose (Fig. 4E), plasma insulin (Fig. 4F), plasma β-hydroxybutyrate (i.e., ketone body) (Fig. 4G), oxygen consumption (Fig. 4H), carbon dioxide production (Fig. 4I), respiratory exchange ratio (Fig. 4J), heat production (Fig. 4K), and food intake (Fig. 4L) under the chow-fed condition.

Overexpression of human GDPD3 increases LysoPA species and promotes TAG accumulation in liver of Western diet-fed mice

LysoPA produced by human GDPD3 can serve as a substrate for TAG synthesis in liver, which is stimulated by high-fat Western diets (28). We investigated whether hepatic overexpression of human GDPD3 in Western diet-fed mice would stimulate hepatic TAG synthesis and accumulation and worsen systemic metabolism. Although the body weight (**Fig. 5A**) was not statistically different from Western diet-fed GFP control mice, liver weight (Fig. 5B) and TAG levels (Fig. 5C) increased in Western diet-fed mice with hepatic human GDPD3 overexpression. Hepatic CE and FC, but not PL, contents were also increased in Western diet-fed mice with hepatic human GDPD3 overexpression (Fig. 5D–F). We then conducted an untargeted lipidomic analysis and found one LysoPA fatty acyl species (16:0) was significantly elevated in the livers of Western diet-fed mice (Fig. 5G). However, similar to results with chow-fed mice (Fig. 4), systemic phenotype (blood glucose, plasma insulin, plasma β-hydroxybutyrate, oxygen consumption, carbon dioxide production, respiratory exchange ratio, heat production, and food intake; data not shown), including blood glucose (Fig. 5H) and insulin (Fig. 5I) homeostasis, was not significantly affected by hepatic GDPD3 overexpression, despite elevated hepatic neutral lipid content (Fig. 5C–E).

Hepatic GDPD3 overexpression increases lipogenesis in Western diet-fed mice

To determine whether increased hepatic TAG in Western diet-fed mice overexpressing human GDPD3 was due to increased FA uptake or de novo hepatic lipogenesis, we incubated primary hepatocytes isolated from Western diet-fed mice with: *1*) [^{14}C]palmitic acid to measure FA uptake, *2*) [^{3}H]oleic acid to measure FA incorporation into hepatic neutral lipids, and *3*) [^{14}C]acetic acid to examine de novo FA synthesis and incorporation into neutral lipids. Hepatocyte [^{14}C]palmitic acid uptake (**Fig. 6A**) was significantly higher in AAV-hGDPD3 mice versus the AAV-GFP control mice consuming a Western diet. [^{3}H]oleic acid incorporation into hepatocyte TAG (Fig. 6B), CE (Fig. 6C), and, to a lesser extent, PL (Fig. 6D) was increased in Western diet-fed AAV-hGDPD3 mice versus AAV-GFP control mice. However, hepatocyte TAG synthesis from [^{14}C]acetic acid was not affected by GDPD3 overexpression (Fig. 6E), suggesting that the primary effect of GDPD3 overexpression was on FA uptake and esterification into TAG (Fig. 6A, B). Newly synthesized CE (Fig. 6F) from [^{14}C]acetic acid was significantly increased in hepatocytes from Western diet-fed AAV-hGDPD3 mice versus AAV-GFP control mice, whereas newly synthesized PL (Fig. 6G) from [^{14}C]acetic acid was reduced in Western diet-fed AAV-hGDPD3 hepatocytes versus control AAV-GFP hepatocytes, likely due to feedback inhibition of PL synthesis (29, 30). Indeed, we did not observe any change of liver PL levels in the steady state between genotypes (Fig. 5F). Human GDPD3 expression in mouse primary hepatocytes used for these experiments was determined by immunoblotting (Fig. 6H).

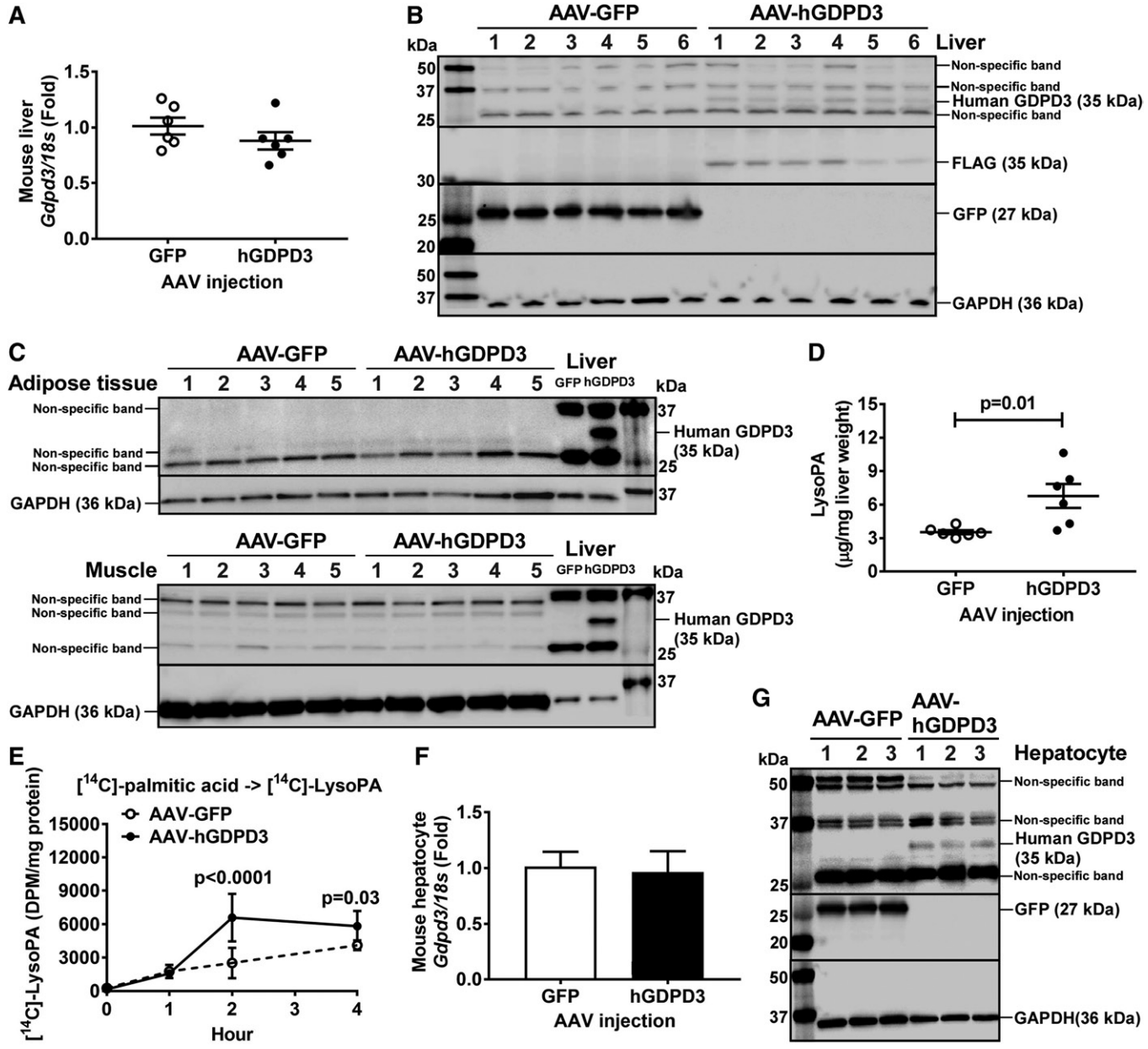

Fig. 3. The effect of human GDPD3 expression on hepatic LysoPA content in chow-fed mice. Six-week-old male mice were treated with the indicated AAV (n = 6 per genotype). Eighteen weeks after AAV injection, livers were collected from chow-fed mice for the measurement of mouse Gdpd3 mRNA (A) and human GDPD3 protein (B); adipose and muscle tissues were also collected for human GDPD3 protein detection (C). D: Chow-fed mouse livers were also used for LysoPA measurement. Six to ten weeks after AAV injection (n = 2 per genotype), primary hepatocytes from chow-fed mice were isolated and incubated with [^{14}C]palmitic acid for 0, 1, 2, and 4 h (n = 6 per time point). E: Newly synthesized [^{14}C]LysoPA was measured as well as the expression of mouse Gdpd3 mRNA (F) and human GDPD3 protein (G). All results are mean ± SEM and analyzed using a two-tailed Student's unpaired *t*-test (A, D, F) or two-way ANOVA with Sidak multiple comparisons (E). DPM, disintegrations per minute.

Patients with macro-steatosis have increased expression of liver GDPD3 mRNA

Human liver samples (n = 54) were histologically evaluated for the degree of macro-steatosis (a single fat vacuole in hepatocytes, displacing the nucleus to the edge of the cell) (31). Twenty-one patients (8 males) with an average body mass index of 35.5 kg/m^2 were classified as having no hepatic steatosis (<5% of hepatocytes containing visible intracellular TAG or macro-steatosis), and 33 patients (9 males) with an average body mass index of 43.6 kg/m^2 had mild (≥5% to <30%), moderate (≥30% to ≤60%), or severe (>60%) macro-steatosis. Patients (n = 33) with mild (≥5% to <30%), moderate (≥30% to ≤60%), or severe (>60%) macro-steatosis had elevated liver TAG (**Fig. 7A**) and CE (Fig. 7B) levels, but not liver FC and PL levels (data not shown), as well as higher liver GDPD3 mRNA levels (Fig. 7C) compared with patients (n = 21) with no hepatic steatosis. In addition, patients with macro-steatosis had increased plasma TAG (Fig. 7D) concentrations, but not plasma CE and FC

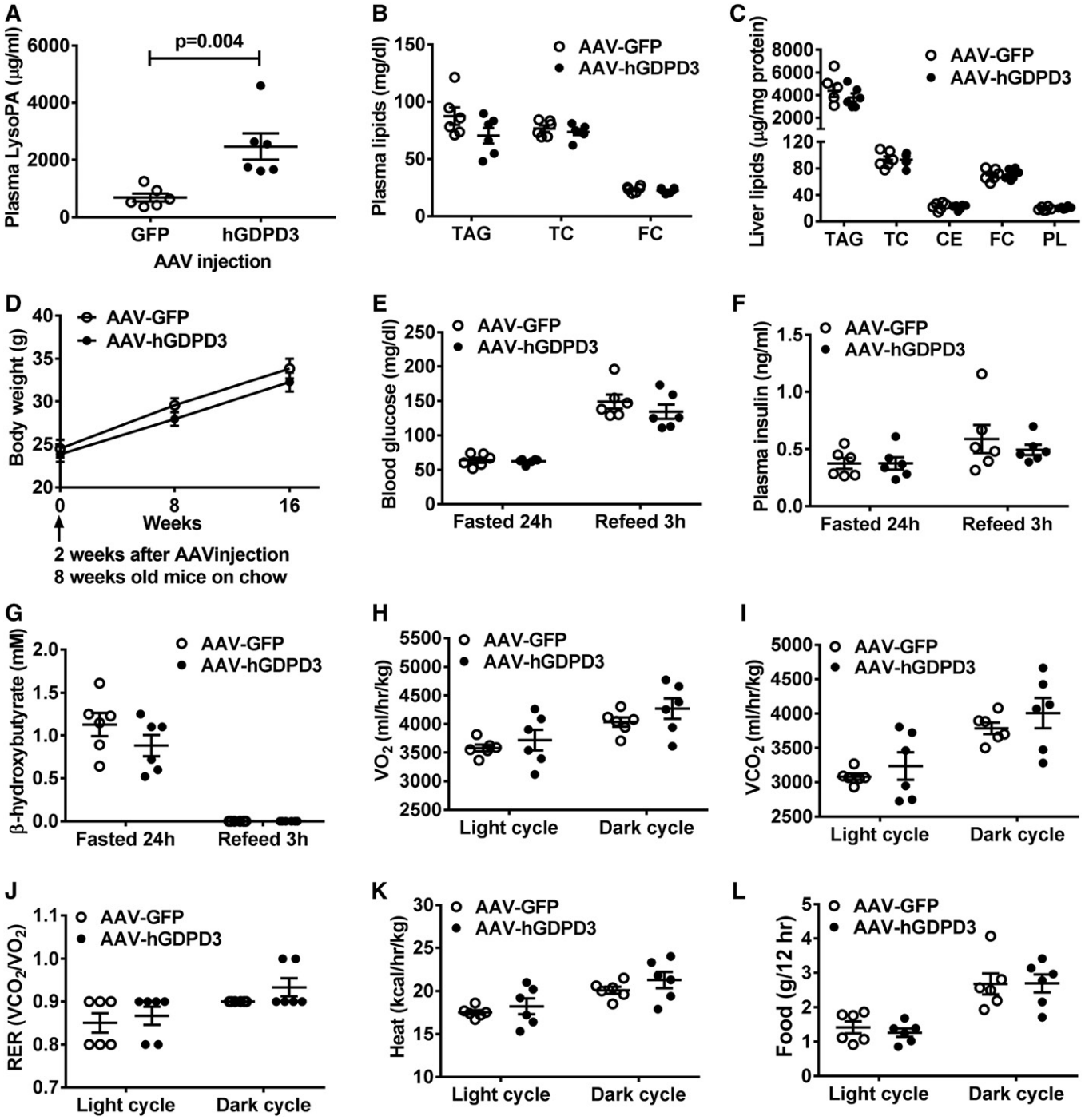

Fig. 4. The effect of human GDPD3 expression on hepatic lipid and systemic metabolism in chow-fed mice. Six-week-old male mice were treated with the indicated AAV (n = 6 per genotype). Eighteen weeks after AAV injection, plasma and livers were collected from chow-fed mice for the measurement of plasma LysoPA (A); plasma TAG, total cholesterol (TC), and FC (B); and liver TAG, TC, CE, FC, and PL (C). D: Chow-fed mouse body weight was measured at 8, 16, and 24 weeks of age. Chow-fed mice (16–18 weeks of age) were used for the measurement of blood glucose (E), plasma insulin (F), β-hydroxybutyrate (G), oxygen consumption (VO_2), (H), carbon dioxide production (VCO_2), (I), respiratory exchange ratio (VCO_2/VO_2) (J), heat production (K), and food intake (L). All results are mean ± SEM and analyzed using a two-tailed Student's unpaired *t*-test.

concentrations (data not shown), compared with patients without hepatic steatosis.

Studies have shown that hepatic steatosis may be present in up to 70% of patients with type 2 diabetes (32, 33). In our study, 15 out of 33 patients with macro-steatosis were diabetics and only 1 out of 21 patients without steatosis was diabetic (Fig. 7E). Indeed, patients with macro-steatosis (n = 33, 15 were diabetics) had increased fasting blood glucose (Fig. 7E) compared with patients without hepatic steatosis (n = 21, one was diabetic). However, there was no

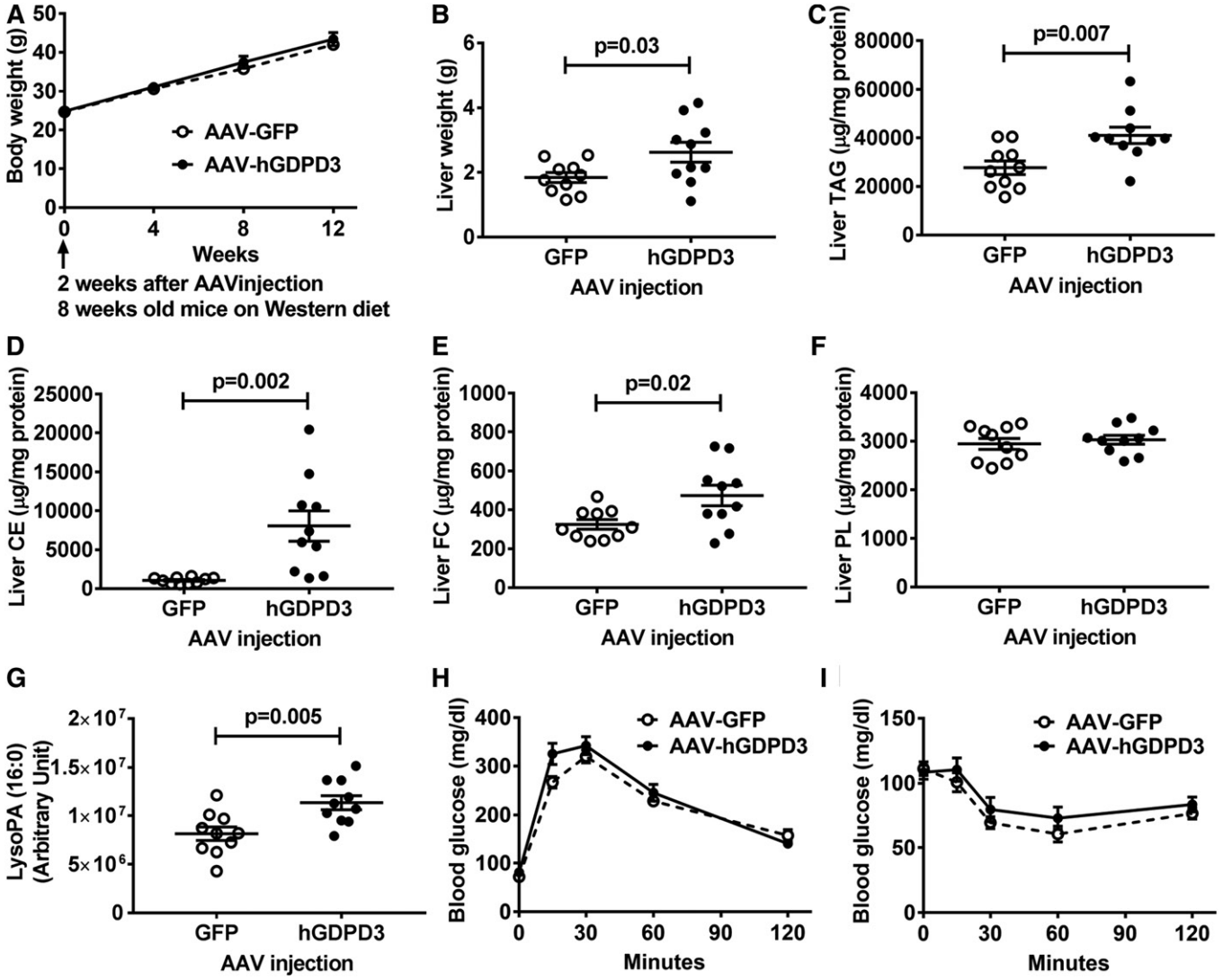

Fig. 5. Overexpression of human GDPD3 in Western diet-fed mice increases hepatic lipid content. Six-week-old male mice were treated with the indicated AAV (n = 10 per genotype) for 2 weeks and then fed a Western diet for 12 weeks. Western diet-fed mice were used for the measurement of body weight at 8, 12, 16, and 20 weeks of age (A). Livers of Western diet-fed mice were collected for the measurement of wet weight (B), TAG (C), CE (D), FC (E), PL (F), and LysoPA (16:0) (G). Glucose tolerance test (H) and insulin tolerance test (I) were performed between 8 and 10 weeks of a Western diet feeding. All results are mean ± SEM and analyzed using a two-tailed Student's unpaired *t*-test.

difference in fasting plasma insulin (Fig. 7F) or homeostatic model assessment of insulin resistance (HOMA-IR; data not shown) due to variability between the two groups.

DISCUSSION

NAFLD encompasses a wide spectrum of liver abnormalities, ranging from benign hepatocellular accumulation of lipids (NAFL or hepatic steatosis), through NASH, to fibrosis and cirrhosis in the absence of excessive consumption of alcohol and hepatitis viral infection (2). The etiology and pathogenesis of NAFLD are poorly understood, reflecting the genetic and environmental heterogeneity of the disease (34). The molecular basis of the metabolic response to dietary fat and its role in NAFLD development remains to be elucidated. In this study, we reported that human GDPD3 overexpression leads to enhanced hepatic steatosis in diet-induced obese mice, and GDPD3 mRNA expression is associated with NAFL in human livers. GDPD3 catalyzed production of LysoPA, a precursor of TAG, and increased hepatic FA uptake and incorporation into esterified neutral lipids, ultimately promoting TAG formation and accumulation, resulting in hepatic steatosis.

Mouse and human GDPD3 were recently cloned and identified as an ER membrane-associated enzyme containing lysophospholipase D activity, converting lysophospholipid to LysoPA in nonhepatic cells (13, 27). Because LysoPA is an intermediate in the glycerol phosphate pathway for TAG biosynthesis (14) and 90% of hepatic TAG is produced through this pathway, we explored whether GDPD3 overexpression increased TAG synthesis. We found that human GDPD3 overexpression stimulated LysoPA production in livers (Fig. 3D) and hepatocytes (Fig. 3E) of chow and

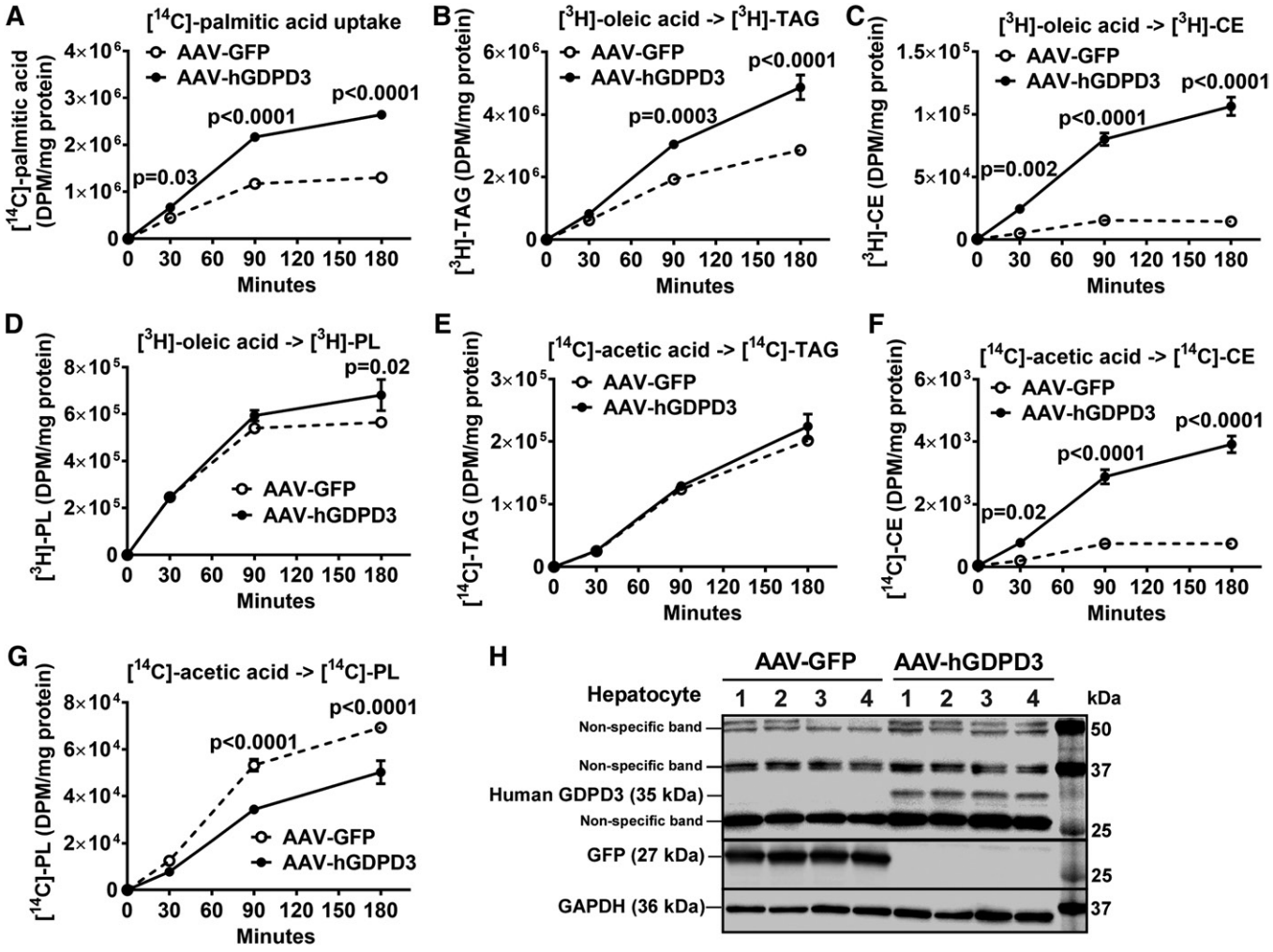

Fig. 6. The effect of human GDPD3 overexpression on lipid synthesis in primary hepatocytes from Western diet-fed mice. Ten to twelve weeks after the indicated AAV injection (n = 2 per genotype), primary hepatocytes were isolated from Western diet-fed mice (8–10 weeks of feeding) and incubated with the indicated radiolabels for up to 180 min (n = 3 per time point). Uptake of [^{14}C]palmitic acid (A), formation of [^{3}H]TAG (B), [^{3}H]CE (C), and [^{3}H]PL (D) from [^{3}H]oleic acid, de novo synthesis of [^{14}C]TAG (E), [^{14}C]CE (F), and [^{14}C]PL (G) from [^{14}C]acetic acid, as well as expression of human GDPD3 protein (H), were measured. All results are mean ± SEM and analyzed using two-way ANOVA with Sidak multiple comparisons (A–G). DPM, disintegrations per minute.

Western diet-fed mice (Fig. 5G). Although increased hepatic LysoPA mediated by human GDPD3 did not affect TAG hemostasis in chow-fed mice (Fig. 4C), it resulted in hepatic lipid accumulation in Western diet-fed mice (Fig. 5C–E). Glycerophosphodiester phosphodiesterase 1 (GDE1) (35), another GDPD family member, hydrolyzes glycerophosphoinositol (36) and glycerophosphocholine (37) to produce glycerol 3-phosphate, which is also an intermediate in the glycerol phosphate pathway for TAG biosynthesis (14). Hepatic *Gde1* overexpression in mice fed a high-fat high-sucrose diet for 7 days induced hepatic TAG accumulation possibly by increasing glycerol 3-phosphate availability for de novo TAG synthesis (35), supporting the concept that the GDPD enzymes may contribute to lipogenesis by providing additional substrate for TAG synthesis from lysophospholipid precursors. The production of LysoPA from glycerol 3-phosphate is controlled by GPAT in the glycerol phosphate pathway for TAG biosynthesis (14). GPAT1 isoform is an outer mitochondrial membrane protein and contributes 30–50% of total GPAT activity in the liver (14). The ER isoform GPAT4 also contributes about 50% of total GPAT activity in the liver (38). Because GPAT4 resides in the ER, where the glycerol phosphate pathway occurs for TAG synthesis, we examined endogenous liver GPAT4 gene expression in chow- and Western diet-fed mice. There was no difference in hepatic Gpat4 mRNA expression between AAV-GFP- and AAV-hGDPD3-injected mice consuming chow or Western diet (data not shown). Thus, we believe that the increased production of hepatic LysoPA in mice injected with AAV-hGDPD3 compared with AAV-GFP controls consuming chow (Fig. 3D) or Western diet (Fig. 5G) was mainly caused by human GDPD3 activity, not by increased GPAT expression.

To determine the relative contribution of exogenous versus de novo synthesized FA used for hepatic TAG biosynthesis in hepatocytes from Western diet-fed mice overexpressing human GDPD3, we used [^{14}C]acetic acid to trace the de novo FA and TAG synthesis, [^{14}C]palmitic acid

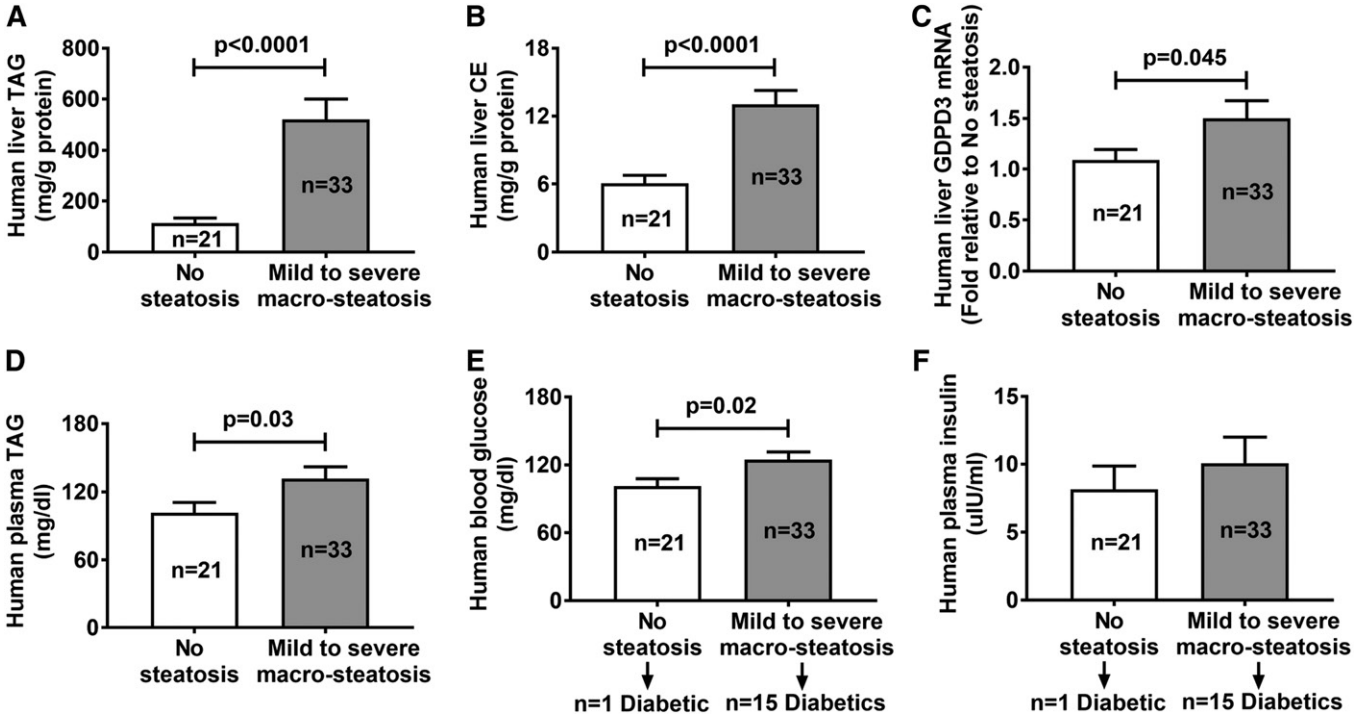

Fig. 7. Liver and plasma lipid profiles in individuals without or with macro-steatosis. Liver biopsy and fasting blood samples were collected from 54 individuals for the measurement of liver TAG (A), liver CE (B), liver GDPD3 mRNA (C), fasting plasma TAG (D), fasting blood glucose (E), and fasting plasma insulin levels (F). All results are mean ± SEM and analyzed using unpaired *t*-test with Welch's correction.

to monitor cellular FA uptake, and [^{3}H]oleic acid to follow FA esterification into TAG. Newly synthesized TAG from [^{14}C]acetic acid was not affected by human GDPD3 overexpression (Fig. 6E), indicating that de novo lipogenesis is unlikely causing hepatic TAG accumulation in AAV-hGDPD3 mice on Western diet. In addition, mRNA expression of Acc1 and Fasn, two enzymes that regulate de novo FA synthesis (39, 40), was unaffected in Western diet-fed mouse liver expressing human GDPD3 (data not shown). However, we observed an increase in hepatocyte [^{14}C] palmitic acid uptake (Fig. 6A) and [^{3}H]oleic acid incorporation into TAG (Fig. 6B) and CE (Fig. 6C) in human GDPD3-overexpressing hepatocytes isolated from Western diet-fed mice. Donnelly et al. (41) used a multiple-stable-isotope approach demonstrating that liver fatty acyl groups consisted of 60% of free FA influx from adipose tissue (lipolysis), 15% from the diet, and 25% of de novo lipogenesis (FA synthesis from acetate). In addition, Duarte et al. (42) used a deuterated water NMR approach and reported that high-fat diet-induced hepatic TAG accumulation was mediated through re-esterification of existing or ingested lipids, not de novo lipogenesis. Therefore, two components are required for our model: *1*) GDPD3 increases LysoPA flux, and *2*) a high-fat diet provides FA substrate. Through acylation and dephosphorylation reactions in the glycerol phosphate pathway, LysoPA is converted to TAG for hepatic neutral lipid storage and accumulation (Fig. 1).

How does overexpression of GDPD3 increase hepatic FA uptake (Fig. 6A)? PPARα and PPARγ are ligand-activated nuclear receptors that transcriptionally regulate glucose and lipid metabolism in multiple metabolically active organs (43). PPARγ expression is low in liver but elevated in NAFLD (44–46). Deletion of PPARγ in mouse hepatocytes protects against hepatosteatosis (45, 47). Prior studies demonstrated that PPARγ activation induces the expression of genes involved in FA uptake, such as CD36/FA translocase (48) and FATPs (49), leading to increased hepatic TAG synthesis and storage. Because LysoPA is a well-known PPARγ ligand (50–52), we hypothesize that PPARγ is the functional receptor for LysoPA produced by human GDPD3, enhancing hepatic steatosis via increased FA uptake through CD36 and/or FATPs (Fig. 1). We found that total and membrane-associated hepatic CD36 protein expression was not affected by overexpression of human GDPD3 (data not shown). We will focus future studies on investigating the effect of human GDPD3 overexpression on liver PPARγ activation and FA uptake via FATPs, such as FATP2 (53) and FATP5 (54). Lastly, PPARα is the predominant PPAR isoform in the liver and regulates hepatic FA metabolism by inducing expression of genes involved in FA oxidation, including Cpt1 and Cpt2 (55). CPT1α is the primary Cpt1 isoform expressed in liver (55). LysoPA has not previously been identified as a PPARα ligand, and there was no difference in the gene expression of hepatic Pparα, Cpt1α, and Cpt2 between Western diet-fed AAV-GFP- and AAV-hGDPD3-injected mice (data not shown), suggesting that human GDPD3 overexpression did not affect hepatic FA oxidation.

Our study has potential limitations. We did not perform loss-of-function studies because minimal endogenous hepatic Gdpd3 gene expression in chow-fed C57BL/6J mice

(Fig. 2A) reduces the dynamic range to observe functional differences between the wild-type and Gdpd3 knockdown livers. In addition, global Gdpd3 knockout mice have no apparent visible abnormalities as assessed by hematoxylin- and eosin-stained liver sections compared with age- and gender-matched controls (56). Feeding global Gdpd3 knockout mice a high-fat diet is required to determine whether inhibition of GDPD3 contributes significantly to prevention of hepatic steatosis. Another limitation is that hepatic steatosis in Western diet-fed mice was achieved with supraphysiological hepatic overexpression of human GDPD3. It remains unknown whether the relatively small increase in hepatic GDPD3 mRNA in humans with liver steatosis (Fig. 7C) is sufficient to contribute to enhanced liver TAG accumulation.

In summary, our findings indicate that GDPD3 overexpression increases LysoPA availability and hepatic FA flux, promoting TAG biosynthesis and accumulation through the ER glycerol phosphate pathway in mouse hepatocytes/livers. Although our results rely on GDPD3 overexpression, our human data suggest that increased dietary FA availability may be responsible for increased transcription of hepatic GDPD3 in humans with hepatic steatosis and identify GDPD3 as a potential contributor to Western diet-induced hepatic steatosis.

Data availability

The data supporting the findings of this study are available within the article. Derived data supporting the findings of this study are available from the corresponding author (C-C.C.K.) on request.

The authors gratefully acknowledge services provided by the Lipid, Lipoprotein, and Atherosclerosis Analysis Laboratory of the Department of Internal Medicine/Section on Molecular Medicine; the Center on Diabetes, Obesity, and Metabolism; the Proteomics and Metabolomics Shared Resource (supported in part by National Cancer Institute Grant P30 CA121291-37); and the Cell and Viral Vector Core Laboratory (supported in part by National Cancer Institute Grant P30 CA121291-37) of the Comprehensive Cancer Center at the Wake Forest School of Medicine.

REFERENCES

1. Ludwig, J., T. R. Viggiano, D. B. McGill, and B. J. Oh. 1980. Nonalcoholic steatohepatitis: Mayo Clinic experiences with a hitherto unnamed disease. *Mayo Clin. Proc.* **55:** 434–438.
2. Rinella, M. E. 2015. Nonalcoholic fatty liver disease: a systematic review. *JAMA.* **313:** 2263–2273.
3. Hodson, L., and P. J. Gunn. 2020. Publisher correction: The regulation of hepatic fatty acid synthesis and partitioning: the effect of nutritional state. *Nat. Rev. Endocrinol.* **16:** 340.
4. Coleman, R. A., and D. P. Lee. 2004. Enzymes of triacylglycerol synthesis and their regulation. *Prog. Lipid Res.* **43:** 134–176.
5. Gimeno, R. E., and J. Cao. 2008. Mammalian glycerol-3-phosphate acyltransferases: new genes for an old activity. *J. Lipid Res.* **49:** 2079–2088.
6. Shindou, H., D. Hishikawa, T. Harayama, K. Yuki, and T. Shimizu. 2009. Recent progress on acyl CoA: lysophospholipid acyltransferase research. *J. Lipid Res.* **50(Suppl):** S46–S51.
7. Zhang, P., and K. Reue. 2017. Lipin proteins and glycerolipid metabolism: roles at the ER membrane and beyond. *Biochim. Biophys. Acta Biomembr.* **1859:** 1583–1595.
8. Yen, C. L., S. J. Stone, S. Koliwad, C. Harris, and R. V. Farese, Jr. 2008. DGAT enzymes and triacylglycerol biosynthesis. *J. Lipid Res.* **49:** 2283–2301.
9. Hodson, L., and P. J. Gunn. 2019. The regulation of hepatic fatty acid synthesis and partitioning: the effect of nutritional state. *Nat. Rev. Endocrinol.* **15:** 689–700.
10. Fisher, E., C. Almaguer, R. Holic, P. Griac, and J. Patton-Vogt. 2005. Glycerophosphocholine-dependent growth requires Gde1p (YPL110c) and Git1p in Saccharomyces cerevisiae. *J. Biol. Chem.* **280:** 36110–36117.
11. Bishop, A. C., S. Ganguly, N. V. Solis, B. M. Cooley, M. I. Jensen-Seaman, S. G. Filler, A. P. Mitchell, and J. Patton-Vogt. 2013. Glycerophosphocholine utilization by Candida albicans: role of the Git3 transporter in virulence. *J. Biol. Chem.* **288:** 33939–33952.
12. Corda, D., M. G. Mosca, N. Ohshima, L. Grauso, N. Yanaka, and S. Mariggio. 2014. The emerging physiological roles of the glycerophosphodiesterase family. *FEBS J.* **281:** 998–1016.
13. Ohshima, N., T. Kudo, Y. Yamashita, S. Mariggio, M. Araki, A. Honda, T. Nagano, C. Isaji, N. Kato, D. Corda, et al. 2015. New members of the mammalian glycerophosphodiester phosphodiesterase family: GDE4 and GDE7 produce lysophosphatidic acid by lysophospholipase D activity. *J. Biol. Chem.* **290:** 4260–4271.
14. Takeuchi, K., and K. Reue. 2009. Biochemistry, physiology, and genetics of GPAT, AGPAT, and lipin enzymes in triglyceride synthesis. *Am. J. Physiol. Endocrinol. Metab.* **296:** E1195–E1209.
15. Key, C. C., M. Liu, C. L. Kurtz, S. Chung, E. Boudyguina, T. A. Dinh, A. Bashore, P. E. Phelan, B. I. Freedman, T. F. Osborne, et al. 2017. Hepatocyte ABCA1 deletion impairs liver insulin signaling and lipogenesis. *Cell Rep.* **19:** 2116–2129.
16. Narváez-Rivas, M., N. Vu, G. Y. Chen, and Q. Zhang. 2017. Off-line mixed-mode liquid chromatography coupled with reversed phase high performance liquid chromatography-high resolution mass spectrometry to improve coverage in lipidomics analysis. *Anal. Chim. Acta.* **954:** 140–150.
17. Jelenik, T., K. Kaul, G. Sequaris, U. Flogel, E. Phielix, J. Kotzka, B. Knebel, P. Fahlbusch, T. Horbelt, S. Lehr, et al. 2017. Mechanisms of insulin resistance in primary and secondary nonalcoholic fatty liver. *Diabetes.* **66:** 2241–2253.
18. Nguyen, T. M., J. K. Sawyer, K. L. Kelley, M. A. Davis, and L. L. Rudel. 2012. Cholesterol esterification by ACAT2 is essential for efficient intestinal cholesterol absorption: evidence from thoracic lymph duct cannulation. *J. Lipid Res.* **53:** 95–104.
19. Lowry, O. H., N. J. Rosebrough, A. L. Farr, and R. J. Randall. 1951. Protein measurement with the Folin phenol reagent. *J. Biol. Chem.* **193:** 265–275.
20. Yamada, T., T. Uchikata, S. Sakamoto, Y. Yokoi, E. Fukusaki, and T. Bamba. 2013. Development of a lipid profiling system using reverse-phase liquid chromatography coupled to high-resolution mass spectrometry with rapid polarity switching and an automated lipid identification software. *J. Chromatogr. A.* **1292:** 211–218.
21. Shores, N. J., K. Link, A. Fernandez, K. R. Geisinger, M. Davis, T. Nguyen, J. Sawyer, and L. Rudel. 2011. Non-contrasted computed tomography for the accurate measurement of liver steatosis in obese patients. *Dig. Dis. Sci.* **56:** 2145–2151.
22. Franzén, L. E., M. Ekstedt, S. Kechagias, and L. Bodin. 2005. Semiquantitative evaluation overestimates the degree of steatosis in liver biopsies: a comparison to stereological point counting. *Mod. Pathol.* **18:** 912–916.
23. Kleiner, D. E., Brunt, E. M., Van Natta, M., Behling, C., Contos, M. J., Cummings, O. W., Ferrell, L. D., Liu, Y. C., Torbenson, M. S., Unalp-Arida, et al. 2005. Design and validation of a histological scoring system for nonalcoholic fatty liver disease. *Hepatology.* **41:** 1313–1321.
24. Livak, K. J., and T. D. Schmittgen. 2001. Analysis of relative gene expression data using real-time quantitative PCR and the 2(-Delta Delta C(T)) method. *Methods.* **25:** 402–408.
25. Guan, H. P., J. L. Goldstein, M. S. Brown, and G. Liang. 2009. Accelerated fatty acid oxidation in muscle averts fasting-induced hepatic steatosis in SJL/J mice. *J. Biol. Chem.* **284:** 24644–24652.
26. Liang, G., J. Yang, J. D. Horton, R. E. Hammer, J. L. Goldstein, and M. S. Brown. 2002. Diminished hepatic response to fasting/refeeding and liver X receptor agonists in mice with selective deficiency of sterol regulatory element-binding protein-1c. *J. Biol. Chem.* **277:** 9520–9528.
27. Rahman, I. A., K. Tsuboi, Z. Hussain, R. Yamashita, Y. Okamoto, T. Uyama, N. Yamazaki, T. Tanaka, A. Tokumura, and N. Ueda. 2016. Calcium-dependent generation of N-acylethanolamines and

lysophosphatidic acids by glycerophosphodiesterase GDE7. *Biochim. Biophys. Acta.* **1861:** 1881–1892.
28. Ferramosca, A., and V. Zara. 2014. Modulation of hepatic steatosis by dietary fatty acids. *World J. Gastroenterol.* **20:** 1746–1755.
29. Shigeura, H. T., A. C. Hen, and K. Hoogsteen. 1975. Drug-induced suppression of phospholipid synthesis in HeLa cells by inhibition of choline uptake. *Biochim. Biophys. Acta.* **388:** 180–187.
30. Viktorova, E. G., J. A. Nchoutmboube, L. A. Ford-Siltz, E. Iverson, and G. A. Belov. 2018. Phospholipid synthesis fueled by lipid droplets drives the structural development of poliovirus replication organelles. *PLoS Pathog.* **14:** e1007280.
31. Ahmed, E. A., A. M. El-Badry, F. Mocchegiani, R. Montalti, A. E. A. Hassan, A. A. Redwan, and M. Vivarelli. 2018. Impact of Graft Steatosis on Postoperative Complications after Liver Transplantation. *Surg. J. (N.Y.).* **4:** e188–e196.
32. Williamson, R. M., Price, J. F., Glancy, S., Perry, E., Nee, L. D., Hayes, P. C., Frier, B. M., Van Look, L. A., Johnston, G. I., Reynolds, et al. 2011. Prevalence of and risk factors for hepatic steatosis and nonalcoholic Fatty liver disease in people with type 2 diabetes: the Edinburgh Type 2 Diabetes Study. *Diabetes Care.* **34:** 1139–1144.
33. Targher, G., L. Bertolini, R. Padovani, S. Rodella, R. Tessari, L. Zenari, C. Day, and G. Arcaro. 2007. Prevalence of nonalcoholic fatty liver disease and its association with cardiovascular disease among type 2 diabetic patients. *Diabetes Care.* **30:** 1212–1218.
34. Hooper, A. J., L. A. Adams, and J. R. Burnett. 2011. Genetic determinants of hepatic steatosis in man. *J. Lipid Res.* **52:** 593–617.
35. Hui, S. T., B. W. Parks, E. Org, F. Norheim, N. Che, C. Pan, L. W. Castellani, S. Charugundla, D. L. Dirks, N. Psychogios, et al. 2015. The genetic architecture of NAFLD among inbred strains of mice. *eLife.* **4:** e05607.
36. Zheng, B., C. P. Berrie, D. Corda, and M. G. Farquhar. 2003. GDE1/MIR16 is a glycerophosphoinositol phosphodiesterase regulated by stimulation of G protein-coupled receptors. *Proc. Natl. Acad. Sci. USA.* **100:** 1745–1750.
37. Gallazzini, M., J. D. Ferraris, and M. B. Burg. 2008. GDPD5 is a glycerophosphocholine phosphodiesterase that osmotically regulates the osmoprotective organic osmolyte GPC. *Proc. Natl. Acad. Sci. USA.* **105:** 11026–11031.
38. Zhang, C., D. E. Cooper, T. J. Grevengoed, L. O. Li, E. L. Klett, J. M. Eaton, T. E. Harris, and R. A. Coleman. 2014. Glycerol-3-phosphate acyltransferase-4-deficient mice are protected from diet-induced insulin resistance by the enhanced association of mTOR and rictor. *Am. J. Physiol. Endocrinol. Metab.* **307:** E305–E315.
39. Vacca, M., M. Allison, J. L. Griffin, and A. Vidal-Puig. 2015. Fatty acid and glucose sensors in hepatic lipid metabolism: implications in NAFLD. *Semin. Liver Dis.* **35:** 250–261.
40. Bechmann, L. P., R. A. Hannivoort, G. Gerken, G. S. Hotamisligil, M. Trauner, and A. Canbay. 2012. The interaction of hepatic lipid and glucose metabolism in liver diseases. *J. Hepatol.* **56:** 952–964.
41. Donnelly, K. L., C. I. Smith, S. J. Schwarzenberg, J. Jessurun, M. D. Boldt, and E. J. Parks. 2005. Sources of fatty acids stored in liver and secreted via lipoproteins in patients with nonalcoholic fatty liver disease. *J. Clin. Invest.* **115:** 1343–1351.
42. Duarte, J. A., F. Carvalho, M. Pearson, J. D. Horton, J. D. Browning, J. G. Jones, and S. C. Burgess. 2014. A high-fat diet suppresses de novo lipogenesis and desaturation but not elongation and triglyceride synthesis in mice. *J. Lipid Res.* **55:** 2541–2553.
43. Ferré, P. 2004. The biology of peroxisome proliferator-activated receptors: relationship with lipid metabolism and insulin sensitivity. *Diabetes.* **53 (Suppl. 1):** S43–S50.
44. Yamazaki, T., S. Shiraishi, K. Kishimoto, S. Miura, and O. Ezaki. 2011. An increase in liver PPARgamma2 is an initial event to induce fatty liver in response to a diet high in butter: PPARgamma2 knockdown improves fatty liver induced by high-saturated fat. *J. Nutr. Biochem.* **22:** 543–553.
45. Morán-Salvador, E., M. Lopez-Parra, V. Garcia-Alonso, E. Titos, M. Martinez-Clemente, A. Gonzalez-Periz, C. Lopez-Vicario, Y. Barak, V. Arroyo, and J. Claria. 2011. Role for PPARgamma in obesity-induced hepatic steatosis as determined by hepatocyte- and macrophage-specific conditional knockouts. *FASEB J.* **25:** 2538–2550.
46. Pettinelli, P., and L. A. Videla. 2011. Up-regulation of PPAR-gamma mRNA expression in the liver of obese patients: an additional reinforcing lipogenic mechanism to SREBP-1c induction. *J. Clin. Endocrinol. Metab.* **96:** 1424–1430.
47. Matsusue, K., M. Haluzik, G. Lambert, S. H. Yim, O. Gavrilova, J. M. Ward, B. Brewer, Jr., M. L. Reitman, and F. J. Gonzalez. 2003. Liver-specific disruption of PPARgamma in leptin-deficient mice improves fatty liver but aggravates diabetic phenotypes. *J. Clin. Invest.* **111:** 737–747.
48. Zhou, J., M. Febbraio, T. Wada, Y. Zhai, R. Kuruba, J. He, J. H. Lee, S. Khadem, S. Ren, S. Li, et al. 2008. Hepatic fatty acid transporter Cd36 is a common target of LXR, PXR, and PPARgamma in promoting steatosis. *Gastroenterology.* **134:** 556–567.
49. Schaiff, W. T., I. Bildirici, M. Cheong, P. L. Chern, D. M. Nelson, and Y. Sadovsky. 2005. Peroxisome proliferator-activated receptor-gamma and retinoid X receptor signaling regulate fatty acid uptake by primary human placental trophoblasts. *J. Clin. Endocrinol. Metab.* **90:** 4267–4275.
50. McIntyre, T. M., A. V. Pontsler, A. R. Silva, A. St Hilaire, Y. Xu, J. C. Hinshaw, G. A. Zimmerman, K. Hama, J. Aoki, H. Arai, et al. 2003. Identification of an intracellular receptor for lysophosphatidic acid (LPA): LPA is a transcellular PPARgamma agonist. *Proc. Natl. Acad. Sci. USA.* **100:** 131–136.
51. Stapleton, C. M., D. G. Mashek, S. Wang, C. A. Nagle, G. W. Cline, P. Thuillier, L. M. Leesnitzer, L. O. Li, J. B. Stimmel, G. I. Shulman, et al. 2011. Lysophosphatidic acid activates peroxisome proliferator activated receptor-gamma in CHO cells that over-express glycerol 3-phosphate acyltransferase-1. *PLoS One.* **6:** e18932.
52. Lodhi, I. J., L. Yin, A. P. Jensen-Urstad, K. Funai, T. Coleman, J. H. Baird, M. K. El Ramahi, B. Razani, H. Song, F. Fu-Hsu, et al. 2012. Inhibiting adipose tissue lipogenesis reprograms thermogenesis and PPARgamma activation to decrease diet-induced obesity. *Cell Metab.* **16:** 189–201.
53. Falcon, A., H. Doege, A. Fluitt, B. Tsang, N. Watson, M. A. Kay, and A. Stahl. 2010. FATP2 is a hepatic fatty acid transporter and peroxisomal very long-chain acyl-CoA synthetase. *Am. J. Physiol. Endocrinol. Metab.* **299:** E384–E393.
54. Doege, H., D. Grimm, A. Falcon, B. Tsang, T. A. Storm, H. Xu, A. M. Ortegon, M. Kazantzis, M. A. Kay, and A. Stahl. 2008. Silencing of hepatic fatty acid transporter protein 5 in vivo reverses diet-induced non-alcoholic fatty liver disease and improves hyperglycemia. *J. Biol. Chem.* **283:** 22186–22192.
55. Schlaepfer, I. R., and M. Joshi. 2020. CPT1A-mediated fat oxidation, mechanisms, and therapeutic potential. *Endocrinology.* **161:** bqz046.
56. Wijayatunge, R., S. R. Holmstrom, S. B. Foley, V. E. Mgbemena, V. Bhargava, G. L. Perez, K. McCrum, and T. S. Ross. 2018. Deficiency of the endocytic protein Hip1 leads to decreased Gdpd3 expression, low phosphocholine, and kypholordosis. *Mol. Cell. Biol.* **38:** e00385-18.